WWW.IJRPR.COM

International Journal of Research Publication and Reviews

Journal homepage: www.ijrpr.com ISSN 2582-7421

Active Controls of MHD Mixed Convection Nanofluid Flow Over a Vertical Plate with Viscous Dissipation

Raphael E. Asibor[1], Akindele M. Okedoye[2,3]

[1]Department of Computer Science/Mathematics, Igbinedion University Okada, Edo State, Nigeria
[2]Department of Mathematics, Covenant University, Ota, Ogun State, Nigeria
[3]Department of Mathematics, Federal University of Petroleum Resources, Effurun, Nigeria
DOI: https://doi.org/10.55248/gengpi.2023.4207

A B S T R A C T

A significant and developing area of fluid dynamics is flow control. Due to its frequent occurrence in engineering and industrial applications, it means a tiny modification of a configuration providing an ideally big engineering benefit, such as drag reduction, lift enhancement, mixing enhancement, or noise reduction. MHD Active and Passive Controls Mixed convection nanofluid flow, including buoyant forces and viscous dissipation in the presence of chemical reaction, over a vertical plate. Using self-similarity variables, the system of highly nonlinear partial differential equations is first converted to a system of ordinary differential equations. The Richardson extrapolation enhancer and the midrich algorithm are then used to solve the resulting boundary problem system. We applied realistic Prandtl numbers of 0.71, which correspond to air at a temperature of 25 °C and a single atmospheric pressure. 2.62 was chosen as the Schmidt number to reflect the diffusing chemical species of propyl benzene. When the contributions of buoyant forces, viscous dissipation, and the presence of chemical reaction are taken to be zero, existing results are compared with our numerical result to validate it. Graphs and tables were used to show the impact of different controlling parameters, and a thorough discussion followed.

Keywords: Mixed convection; Jeffrey fluid; Nanoparticles; passive controls of nanoparticles; Nonlinear stretching surface; Newtonian

MSC Subject Classification: 76A05, 76B75, 76D05

Nomenclature

x, y	flow axis	Greek Symbol	
u, v	Velocity component along x and y-axis	ρ	fluid density
T	Non-dimensional Temperature field	σ	Electrical conductivity
C	Non-dimensional Species concentration field	ψ	stream function
g	Acceleration due to gravity	**Dimensionless group**	
B_0	Magnetic field of uniform strength	Bi	Convective heat transfer
T_w	surface temperature	θ	dimensionless temperature
T_∞	ambient temperature	ϕ	dimensionless concentration
C_w	surface concentration	Gr	Grashof number for mass transfer
C_∞	ambient concentration	N	buoyancy ratio
β_t	Volumetric coefficient of thermal expansion	λ	Chemical reaction parameter
β_c	Volumetric coefficient of mass expansion	α	heat generation parameter
k	thermal conductivity	M	Magnetic parameter
c_p	specific heat capacity at constant pressure	Pr	Prandtl number
D	Molecular diffusivity	Sc	Schmidt number
U_∞	ambient velocity	Nu	Nusselt number
Q	Heat source/sink parameter	Sh	Sherwood number
G	reactivity parameter	**Subscript**	
		∞	ambient condition
		w	wall condition

Introduction

Over the past few decades, flow analysis of non-Newtonian fluids has drawn a lot of interest. This is due to the fact that it is used in engineering and other industrial applications. These liquids are particularly used in the food industry, metal and plastic industries, chemical and nuclear industries, bioengineering, and polymeric liquids, among other industries. It is impossible to distinguish all non-Newtonian fluid expressions by using a single relationship due to their various features. Thus, in line with the properties of non-Newtonian fluids, several non-Newtonian relations are proposed. A significant and quickly developing area of fluid dynamics is flow control. It suggests a tiny adjustment to a configuration that serves a larger-than-ideal engineering benefit, such as noise reduction, lift increase, drag reduction, or drag reduction. Passive gadgets may be able to effect this transformation. Turbulators and roughness elements are examples of passive devices that are constant and by definition do not require any energy. According to Yousefi and Saleh (2015), passive flow control methods don't need supplemental power or a control loop. Geometric sculpting, the use of vortex generators, and the application of longitudinal grooves or riblets to the surfaces of airfoils are all examples of passive approaches. Materials and devices that improve damping, strength, and stiffness make up passive control systems. The most prevalent devices in this class often function according to concepts like fluid deformation and viscoelastic solid deformation, frictional sliding, and metal yielding in the scenario studied in this chapter. A passive dissipation device produces the control force by using the structure's motion (no external power source needed). Following, a specific emphasis will be placed on fluid viscous dampers, or FVDs, and their design optimization, which is a time-consuming task. Lubrication, viscometry, and extrusion all involve the flow of liquids, therefore viscous heating is a significant issue. The proportion of heat generated by viscous dissipation to heat carried by molecular conduction is known as the Brinkman number, and it has no dimensions. i.e., the proportion of viscous heating to outside heating. The higher the value, the slower the heat created by viscous dissipation will be transferred and hence, the greater the temperature increase. Therefore, the Brinkman number, which is the ratio of viscous dissipation to conduction. The impact of relaxation and retardation times are illustrated by the Jeffrey fluid model. (Hayat (2016), Muhammad (2017), Turkyilmazoglu M, Pop I (2013), Abbasi et al. (2015), Alsaedi, Iqbal, Mustafa, Hayat (2012)). A subfield of electromagnetic field dynamics known as magnetohydrodynamics, or MHD, focuses on the dynamics of matter moving in the field, particularly when the field is modified by currents created in the matter via induction and the field and dynamics equations are coupled. It specifically addresses conducting fluids, whether they be liquid or gaseous, in which certain postulates for simplification are recognized. These include, in general, ignoring the Maxwell displacement current and treating the fluid as a continuum devoid of mean-free-path effects. Although it differs from the closely related plasma dynamics, where these postulates are relaxed, a sizable intermediate area still exists that can receive a similar treatment. MHD was first used to solve problems in astrophysics and geophysics, where it is still crucial today, but it has more recently been used to solve the issue of fusion power, where the solution involves the electromagnetic creation and confinement of hot plasmas because material walls would otherwise be destroyed. Solar structure, particularly in its outer layers, the solar wind that covers the earth and other planets, and interstellar magnetic fields are all examples of astrophysical issues. Planetary magnetism, which is caused by deep-space currents on the planet, is the main geophysical challenge that hasn't been satisfactorily resolved.

In order to take into account buoyant forces, viscous dissipation, and the existence of chemical reaction, we revisit Hayat (2017). When the contributions of buoyant forces, viscous dissipation, and the presence of chemical reaction are taken to be zero, we validate our results..

Governing equations

Let's take into consideration the continuous flow of Jeffrey nanofluid through a nonlinear stretching surface under conditions of both zero and nonzero nanoparticle mass flux. According to Hayat, Mahomed, Asghar (2005), Khan, Maqbool, Hayat (2006), Noor, Kechil, Hashim (2010), Hayat, Qasim and Mesloub (2011), and Hayat, Shehzad, Alsaedi (2012), a non-uniform magnetic field of strength B_0 is imposed in the y-direction. The absence of the induced magnetic field is justified by the low magnetic Reynolds number. The Brownian motion and thermophoresis-subject nanofluid model is used. The sheet is stretched along the x-axis in this instance, and the y-axis is parallel to the x-axis. With a and $n > 0$ as constants, $U_w(x) = ax^n$ is the stretching velocity. The momentum equation accounts for the effects of buoyancy and density fluctuation (Boussinesq approximation). Additionally, there is no applied electric field and no consideration is given to any of the Hall effects or Joule heating (Figure 1). We presume that the induced magnetic field is insignificant because the majority of industrial fluids have relatively low magnetic Reynolds numbers.

Let the x-axis follow the plate's direction, and the y-axis run perpendicular to it. According to Kothandapani and Srinivas (2008), Alsaedi, Iqbal, Mustafa and Hayat (2012), Hayat et al. (2016), and Hayat (2017), the governing equations can be written as follows:

$$\frac{\partial u}{\partial x} + \frac{\partial v}{\partial y} = 0 \tag{1}$$

$$u\frac{\partial u}{\partial x} + v\frac{\partial u}{\partial y} = \frac{\nu}{1+\gamma_1}\left(\frac{\partial^2 u}{\partial y^2} + \lambda_2\left(u\frac{\partial^3 u}{\partial x \partial y^2} + \frac{\partial u}{\partial x}\frac{\partial^2 u}{\partial y^2} - \frac{\partial u}{\partial y}\frac{\partial^2 u}{\partial x \partial y} + v\frac{\partial^2 u}{\partial y^2}\right)\right) \quad - \frac{\sigma B^2}{\rho_f}u + \frac{g\beta_t(x)}{\rho_f}(T - T_\infty) + \frac{g\beta_c(x)}{\rho_f}(C - C_\infty), \tag{2}$$

$$u\frac{\partial T}{\partial x} + v\frac{\partial T}{\partial y} = k\frac{\partial^2 T}{\partial y^2} + \frac{(\rho c)_p}{(\rho c)_f}\left(D_B\left(\frac{\partial T}{\partial y}\frac{\partial C}{\partial y}\right) + \frac{D_T}{T_\infty}\left(\frac{\partial T}{\partial y}\right)^2\right) + Q(T - T_\infty) + \mu\left(\frac{\partial u}{\partial y}\right)^2, \tag{3}$$

$$u\frac{\partial C}{\partial x} + v\frac{\partial C}{\partial y} = D_B\frac{\partial^2 C}{\partial y^2} + \frac{D_T}{T_\infty}\left(\frac{\partial T}{\partial y}\right)^2 - G(C - C_\infty). \tag{4}$$

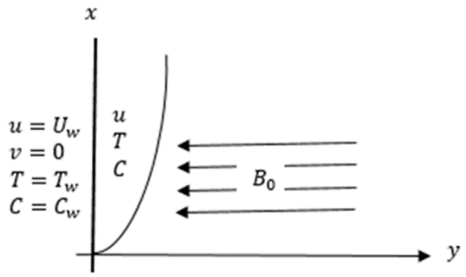

Figure 1. Flow configuration and coordinate system

According to Halim, Haq, and Noor (2017), the conditions at the plate surface and deep into the cold fluid can be expressed as follows:

$$\begin{aligned} &u = U_w = ax, v = 0, T = T_w, D_B\frac{\partial C}{\partial y} + \frac{D_T}{T_\infty}\frac{\partial T}{\partial y} = 0, (passive\ control\ of\ nanoparticles) \quad at\ y = 0 \\ &u \to 0, T \to T_\infty, C \to C_\infty, \qquad as\ y \to \infty, \end{aligned} \tag{5}$$

A similarity solution of Equations (1) – (5) is obtained by defining horizontal and axial component of velocity u and v in terms of independent variable η similar to Hayat (2017)

$$\begin{aligned} u = ax^n f'(\eta), v = -\left(\frac{a\nu(n+1)}{2}\right)^{\frac{1}{2}}(x)^{\frac{n-1}{2}}\left(f(\eta) + \frac{n-1}{n+1}\eta f'(\eta)\right), \eta = \left(\frac{a(n+1)}{2\nu}\right)^{\frac{1}{2}}(x)^{\frac{n-1}{2}}y, \\ \theta(\eta) = \frac{T - T_\infty}{T_w - T_\infty}, \phi(\eta) = \frac{C - C_\infty}{C_\infty}, (passive\ control\ of\ nanoparticles). \end{aligned} \tag{6}$$

Equation (6) perfectly satisfies the continuity equation (1)!

Using similarity variables defined by equation (6), the transformed velocity, temperature and concentration equations are respectively given as

$$\begin{aligned} &\frac{\partial^3}{\partial\eta^3}f(\eta) + \beta\left(\frac{3n-1}{2}\left(\frac{\partial^2}{\partial\eta^2}f(\eta)\right)^2 - \frac{(n+1)}{2}f(\eta)\frac{\partial^4}{\partial\eta^4}f(\eta) + (n-1)\left(\frac{\partial}{\partial\eta}f(\eta)\right)\frac{\partial^3}{\partial\eta^3}f(\eta)\right) \\ &+(1+\gamma)(f(\eta)\frac{\partial^2}{\partial\eta^2}f(\eta) - \frac{2n}{n+1}\left(\frac{\partial}{\partial\eta}f(\eta)\right)^2 - \frac{2}{n+1}\left(Ha^2\frac{\partial}{\partial\eta}f(\eta) - Grc\,\theta(\eta) - Grc\phi(\eta)\right)) = 0, \end{aligned} \tag{7}$$

$$\frac{\partial^2}{\partial\eta^2}\theta(\eta) + Pr\,Pr\left(f(\eta)\frac{\partial}{\partial\eta}\theta(\eta) + Nb\frac{\partial}{\partial\eta}\theta(\eta)\frac{\partial}{\partial\eta}\phi(\eta) + Nt\left(\frac{\partial}{\partial\eta}\theta(\eta)\right)^2 + \frac{\lambda\theta(\eta)}{n+1} + Ec\left(\frac{\partial^2}{\partial\eta^2}f(\eta)\right)^2\right) = 0, \tag{8}$$

$$\frac{\partial^2}{\partial\eta^2}\phi(\eta) + LePrf(\eta)\frac{\partial}{\partial\eta}\phi(\eta) - LePr\delta\frac{\phi(\eta)}{n+1} + \frac{Nt}{Nb}\frac{\partial^2}{\partial\eta^2}\theta(\eta) = 0. \tag{9}$$

And the boundary conditions, after applying the similarity variables becomes

$$f(0) = 0, f'(0) = 1, \theta(0) = 1, \phi(0) = 1 \qquad f'(\infty) \longrightarrow 0, \theta(\infty) \longrightarrow 0, \phi(\infty) \longrightarrow 0 \tag{10}$$

Where the emerging parameters are defined as follows:

$$\begin{aligned} &Grt = \frac{gBt(T_w - T_1)}{a^2x^{2n-1}}, Grc = \frac{gBc(T_w - T_\infty)}{a^2x^{2n-1}}, Nb = \frac{D_B(C_w - C_\infty)(\rho c)_p}{(\rho c)_f\nu}\ Nt = \frac{D_T(T_w - T_1)(\rho c)_p}{(\rho c)_f\nu T_\infty}, \\ &Ha^2 = \frac{\sigma B^2}{\rho a x^{n-1}}, \delta = \frac{G}{a\rho x^{n-1}}; \lambda = \frac{2Q}{\rho_f c_f a x^{n-1}}; Ec = \frac{\mu a^2 x^{2n}}{\rho_f c_f \nu(T_w - T_1)}, Le = \frac{\alpha}{D_B}, \beta = \lambda_2 a x^{n-1} \end{aligned}$$

Flow Rate at the wall

It is necessary to compute other important physical parameters that are relevant to this the discussion under consideration, such as the wall rate transfer in terms skin-friction, the Nusselt number, and the Sherwood number. To determine the total skin-friction, total heat, and total mass transfer rates integration over the entire plate is necessary to obtain the total skin-friction, total heat and mass transfer rate.

Skin friction coefficient and local Nusselt and Sherwood numbers have non-dimensional forms:

$$Re_x^{\frac{1}{2}} C_f = \left(\frac{n+1}{2}\right)^{\frac{1}{2}} \frac{1}{1+\gamma}\left(1+\beta\left(\frac{3n-1}{2}\right)\right) f''(0)$$
$$Re_x^{-\frac{1}{2}} Nu_x = -\left(\frac{n+1}{2}\right)^{\frac{1}{2}} \theta'(0) \quad (11)$$
$$Re_x^{-\frac{1}{2}} Sh_x = -\left(\frac{n+1}{2}\right)^{\frac{1}{2}} \phi'(0)$$

The local Sherwood number for passive control is the same as zero under the passive control condition, therefore:

$$Re_x^{-\frac{1}{2}} Sh_x = -\left(\frac{n+1}{2}\right)^{\frac{1}{2}} \frac{Nt}{Nb} \theta'(0) (16)$$

satisfying the condition in (11) and $Re_x = \frac{U_w x}{\nu}$ represents the local Reynolds number

Method of Solution

In other to secure the solution of the system of equations (7)-(10), we use differential solver, dsolve is maple release 2021 with inbuilt numerical generator madrich with $Ec = 0.4, Grc = 1.5, Grt = 2, Ha = 1, Le = 1.0, Nb = 0.5, Nt = 0.2, Pr = 1.0, \beta = 0.1, \delta = 0.5, \gamma = 0.2, \lambda = 0.3, n = 1.2$as prescribe parameters. The dsolve command with the numeric option on a real-valued two-point boundary value problem (BVP), finds a numerical solution for our system of equations. The bvp under consideration is automatically detected by dsolvesubmethod which uses midrich algorithm is used as solver. The choice of madrich is hinged on its ability to use Richardson extrapolation enhancement or deferred correction enhancement. Computation is performed in both hardware precision and arbitrary precision, by the setting of Digits to 20. This is good enough to maintain both precisions either when Digits is smaller than the hardware precision for the machine or when Digits is larger.

The computations were done by a program which uses a symbolic and computational computer language MAPLE. A step size of $\Delta\eta = 0.001$ was selected to be satisfactory for a convergence criterion of 10^{-7} in nearly all cases. The value of η_∞ was found to each iteration loop by the assignment statement $\eta_\infty = \eta_\infty + \Delta\eta$. The maximum value of η_∞, to each group of parameters is determined when the values of unknown boundary conditions at $\eta = 0$ not change to successful loop with error less than 10^{-7}. The output of the computation is plotted using the ode plot generator odeplot and displayed using Maple plot display, and wall rate transfer is extracted. The graphical results and wall rate transfer are presented below in Figure (2) – (19) and Table (1) and Table (2).

Results and discussion

For our computation in this work, we use realistic values of Prandtl number $Pr = 0.71$ representing air and $Pr = 0.015$ for mercury at a temperature of 25 °C and one atmosphere. Schmidt number (Sc) values of 0.24, 0.64, 0.78, and 2.62 were selected to reflect diffusion of chemical species that are of most common interest in air, such as H_2, H_2O, NH_3, and propyl benzene. Focus is on Grashof number $Gr > 0$, which corresponds to the cooling problem, and solutal Grashof number $Gc > 0$, which are positive values of the buoyancy parameters (which indicates that the chemical species concentration in the free stream region is less than the concentration at the boundary surface). We have compared our results to serve as a standard for our numerical findings the values of $-Re_x^{\frac{1}{2}} C_f$ for varying Deborah Number (β) when $n = 1.0, \gamma = 0.4$ and $Ha = 0.3$ when $Gr = Gc = 0$ with those results obtained by Abbasi et al. (2015) and Hayat et al. (2017), results are found to be in excellent agreement as demonstrated in Table 1.

Table 1: Comparative values of $-Re_x^{\frac{1}{2}} C_f$ for varying b when $n = 1.0, \gamma = 0.4$ and $Ha = 0.3$.

β	Hayat et al. (2017)	Abbasi et al. (02)15	Current Result
0.0	0.88237	0.88237	0.88257044
0.3	1.00605	1.00605	1.00605498
0.6	1.11612	1.11612	1.11612186
1.0	1.24786	1.24786	1.24787382

4.1. Velocity distribution:

The effect of flow governing parameters on velocity distribution were show in Figures 2 – 9. From Figure 2, it was shown that Hartman number adversely affect velocity distribution. This Hartman number is known as Lorentz force which always act in opposite characteristic as velocity thereby brings about an opposing force which in turn reduces the bulk velocity. In Figure 3 and 4, thermal and mass Grashof numbers are seen to aid velocity for cooling problem. It is also observed that for higher Grashof number, a peak exists close to the surface which indicate that maximum velocity occurs in the body of the fluid close to the surface. However, the velocity boundary layer reduces away from the surface with no significant changes far away from the plate surface. The effect of local Deborah number was displayed in Figure 5. From this figure, we observed that as this Local Deborah number increase, the velocity distribution increases close to the surface to about 2units distance from the plate after which the situation is reversed with an increase with increase in Deborah number. While in Figure 6, an increase in heat generation ($\lambda < 0$) reduces the velocity while heat absorption ($\lambda > 0$) increases the velocity boundary layers. Figure 7 shows the variation of velocity distribution with Thermophoresis parameter. It was observed that thermophoretic

parameter aided the velocity distribution. We displayed the effect of Prandtl number on velocity distribution in Figure 8 where we observed that for higher value of Prandtl number, the velocity is reduced and vice-versa. This is so because, higher the Prandtl number is associated with heavy substance with higher resistance to flow hence, the velocity distribution decreases with increase in Prandtl number. Effect of Eckert number on velocity distribution is shown with Figure 9. Increase in Eckert number was observed to bring about increase in velocity within the boundary layer with maximum velocity occurring in the body of the velocity close to the surface.

Table 2: Effect of flow parameters on wall transfer rate for Active (Act.) and Passive (Pass.) Controls

		$Re_x^{\frac{1}{2}}C_f$		$Re_x^{-\frac{1}{2}}Nu_x$		$Re_x^{-\frac{1}{2}}Sh_x$		$f''(0)$		$\phi(0)$
		Act.	Pass.	Act.	Pass.	Act.	Pass.	Act.	Pass.	Pass.
$Ha =$	0.01	1.00070	0.06444	0.39707	0.57782	0.93539	1.44456	0.84	0.05	-0.15
	1.00	0.27791	-0.58994	0.37653	0.47522	0.88365	1.18806	0.23	-0.50	-0.14
	2.00	-1.20398	-1.89900	0.18214	0.15354	0.83995	0.38386	-1.02	-1.60	-0.12
	3.00	-2.74810	-3.28012	-0.16684	-0.27093	0.87173	-0.67733	-2.32	-2.77	-0.09
$Grt =$	0.50	-0.28439	-0.90959	0.33780	0.42326	0.85918	1.05816	-0.24	-0.77	-0.14
	2.00	0.99261	0.05698	0.39714	0.57694	0.93470	1.44235	0.84	0.05	-0.15
	6.00	3.37144	2.36950	0.09224	0.47306	1.17369	1.18265	2.84	2.00	-0.15
	10.00	5.92653	4.78101	-0.67286	-0.09639	1.55890	-0.24096	5.00	4.03	-0.13
$Grc =$	0.00	0.19604	0.11758	0.39168	0.56340	0.88652	1.40849	0.17	0.10	-0.15
	2.00	1.24876	0.03629	0.38669	0.58084	0.95298	1.45209	1.05	0.03	-0.15
	5.00	2.70497	-0.09286	0.23530	0.59931	1.07982	1.49829	2.28	-0.08	-0.15
	10.00	4.89894	-0.32293	-0.22787	0.61597	1.33538	1.53993	4.13	-0.27	-0.16
$\beta =$	0.10	0.99352	0.05794	0.39734	0.57684	0.93457	1.44210	0.84	0.05	-0.15
	0.40	1.06775	0.00112	0.41449	0.58076	0.92004	1.45191	0.67	0.00	-0.15
	0.80	1.08854	-0.09834	0.42543	0.58580	0.90938	1.46450	0.51	-0.05	-0.15
	5.00	0.78059	-2.23507	0.44514	0.68569	0.89139	1.71422	0.05	-0.15	-0.14
$\lambda =$	-3.00	0.74593	-0.27411	1.15191	1.35869	0.65882	3.39671	0.63	-0.23	-0.21
	-1.00	0.86423	-0.11825	0.75239	0.95063	0.80634	2.37659	0.73	-0.10	-0.18
	1.00	1.09753	0.20583	0.14013	0.29392	1.02512	0.73481	0.93	0.17	-0.12
	3.00	1.75214	1.14730	-1.36575	-1.51132	1.51172	-3.77831	1.48	0.97	0.08
$\delta =$	-3.00	1.69907	4.19617	0.53378	-0.43835	-1.20120	-1.09587	1.43	3.54	3.97
	-1.00	1.14797	1.78850	0.43043	0.37706	0.41020	0.94265	0.97	1.51	1.43
	2.00	0.90474	0.05598	0.38020	0.57325	1.28693	1.43312	0.76	0.05	-0.15
	8.00	0.73817	0.08504	0.35464	0.55318	2.18501	1.38295	0.62	0.07	-0.10
$Nb =$	0.05	1.28797	-0.55206	0.55302	0.60539	0.33986	0.15135	1.09	-0.47	-1.60
	0.50	0.91663	0.02781	0.38657	0.56025	0.94652	1.40062	0.77	0.02	-0.15
	1.40	0.98337	0.06432	0.17592	0.55200	0.99227	3.86397	0.83	0.05	-0.05
	5.00	1.18843	0.07864	-0.05457	0.54838	1.01026	13.70943	1.00	0.07	-0.01
$Nt =$	2.00	1.31135	-0.42855	0.17967	0.47721	1.38562	0.11930	1.11	-0.36	-1.40
	4.00	1.36239	-0.99463	0.05081	0.30279	2.36207	0.03785	1.15	-0.84	-2.39
	6.00	1.28013	-1.46654	-0.00575	0.09736	3.16820	0.00811	1.08	-1.24	-2.73
$\gamma =$	0.00	0.82517	0.00272	0.40992	0.58088	0.92672	1.45220	0.70	0.00	-0.15
	0.20	0.99261	0.05698	0.39714	0.57694	0.93470	1.44235	0.84	0.05	-0.15
	0.60	1.30242	0.16016	0.37039	0.57065	0.95023	1.42662	1.10	0.14	-0.15
	1.70	2.03358	0.41022	0.29456	0.55756	0.98975	1.39391	1.72	0.35	-0.14
$Ec =$	0.00	0.93529	0.00133	0.49670	0.64291	0.89906	1.60727	0.79	0.00	-0.16
	1.50	1.15246	0.20590	0.08091	0.41386	1.04620	1.03465	0.97	0.17	-0.12
	3.50	1.52797	0.52402	-0.95023	0.01527	1.40341	0.03818	1.29	0.44	-0.06
	4.00	1.67823	0.64418	-1.47403	-0.19027	1.58344	-0.47567	1.42	0.54	-0.04
$Le =$	0.30	1.22831	0.00034	0.49635	0.59977	0.42083	1.49943	1.04	0.00	-0.20
	1.00	0.99261	0.05698	0.39714	0.57694	0.93470	1.44235	0.84	0.05	-0.15
	1.50	0.90780	0.07213	0.37622	0.56942	1.17307	1.42355	0.77	0.06	-0.13
	3.20	0.75255	0.09459	0.35153	0.55733	1.74773	1.39333	0.63	0.08	-0.10
$Pr =$	0.01	1.97648	0.32679	0.11755	0.11425	0.12784	0.28563	1.67	0.28	-0.33
	0.03	1.90625	0.42010	0.14254	0.13537	0.16902	0.33843	1.61	0.35	-0.25
	0.72	1.10999	0.12988	0.38942	0.50421	0.78001	1.26054	0.94	0.11	-0.15
	2.36	0.70460	-0.12987	0.29396	0.78670	1.51857	1.96674	0.59	-0.11	-0.14

4.2. Energy distribution:

The effect of Lorentz force, heat generation/absorption, thermophoretic Brownian motion and Eckert parameters and, Prandtl number on heat distribution in the boundary layer is shown in Figures 10 – 15. From these figures, we discovered that increase in Lorentz force (Hartman number) brings about increase in temperature as against the scenario in velocity field, as shown in Figure 10. This is because the opposition to velocity resulted into energy loss which is converted to heat thereby increases the bulk temperature of the flow. While from Figure 11, it is shown that heat absorption into the system increases the bulk temperature whereas heat generation reduces the temperature as a result of heat removal from the system. Also at higher value of λ, a peak was observed on the profile which indicate that maximum temperature occur in the body of the fluid close to the surface of the flow. The effect of both Brownian motion and thermophoretic parameters were shown in Figures 12 and 13 respectively. Increase in each of these parameters were seen to enhances the temperature of the system. In Figure 14, increase in Eckert number increases the temperature with maximum temperature occurring in the body of the fluid at higher values of Eckert number. While we discovered from Figure 15 that, the highest temperature is the surface temperature with respect to Prandtl number. Liquid metal was seen to have the highest boundary layer. The thermal boundary layer decrease with increase in Prandtl number.

4.3. Concentration distribution:

In this section, the species concentrations was analysed with respect to various values of reaction parameter Thermophoresis parameter, Lewis and Prandtl numbers. Figure 16 shows that generative chemical reaction ($\delta < 0$) increases the species concentration while destructive chemical reaction ()$\delta > 0$ decrease the concentration as well as the concentration boundary layers. At higher values of generative chemical reaction, a peak was observed in the profile which signifies the occurrence of maximum concentration in the body of the flow close to the surface. Increase in thermophoretic parameter initially decreases the species concentration close to the surface bur reverses at about 1unit from the surface with increase on thermophoretic parameter resulting into increase in species concentration. As shown in Figure 17. Lewis and Prandtl numbers effect on temperature were displayed in Figures 18 and 19 respectively. Both parameters were observed of decreases the species concentration as well as the boundary layer of species concentrations.

4.4 Wall Rate Transfer:

Effect of flow parameters on wall transfer rate for Active (Act.) and Passive (Pass.) Controls is displayed in Table 2. From this table, Lorentz force (Ha) brings about decrease in skin-friction, Nusselt number and Sherwood number respectively. However, the skin-friction corresponding to active control is higher than that in passive control while, Nusselt number and Sherwood number corresponding to passive control were observed to be higher than the case of active control. And increase in Thermal Grashof number result in increase in skin-friction with active control having higher values than the passive control scenario while the wall heat transfer decline in both active and passive controls. In the case of mass transfer at the wall, thermal Grashof number enhances the wall transfer in active control but retard in passive controls. Heat generation/absorption, chemical reaction parameter, local Deborah number are observed to enhance mass transfer at the wall, skin-friction, heat and mass transfer at the wall respectively. While the skin friction, heat transfer respectively. Effect of other flow governing parameters were as displayed in the table which is self-explanatory.

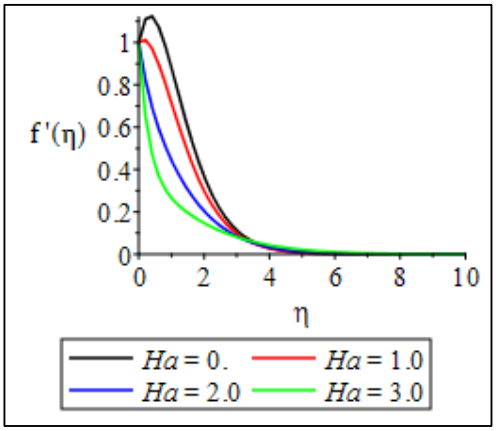

Figure 2: Variation of Velocity Distribution with Hartmann number

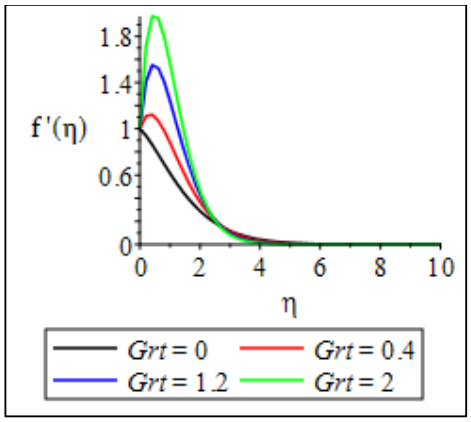

Figure 3: Variation of Velocity Distribution with Thermal Grashof number

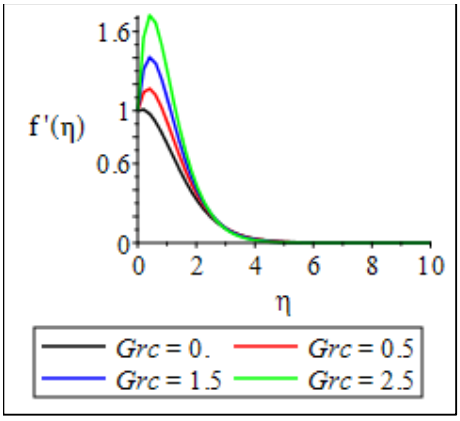

Figure 4: Variation of Velocity Distribution with Mass Grashof number

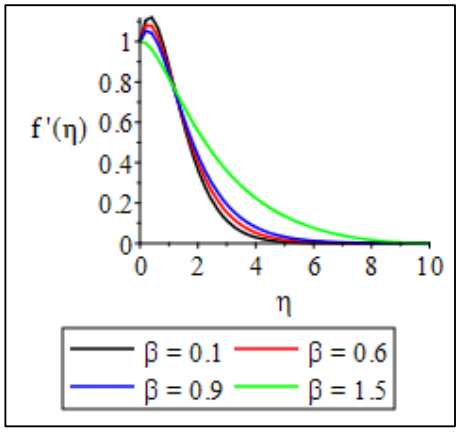

Figure 5: Variation of Velocity Distribution with Deborah number

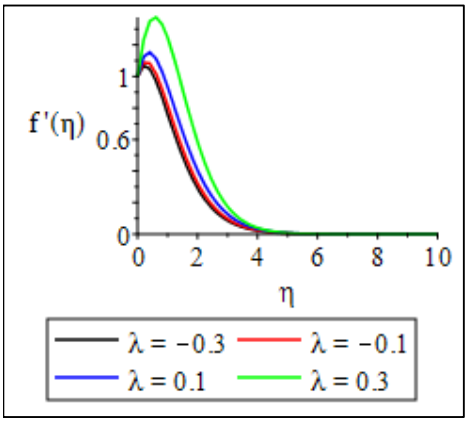

Figure 6: Variation of Velocity Distribution with Heat generation

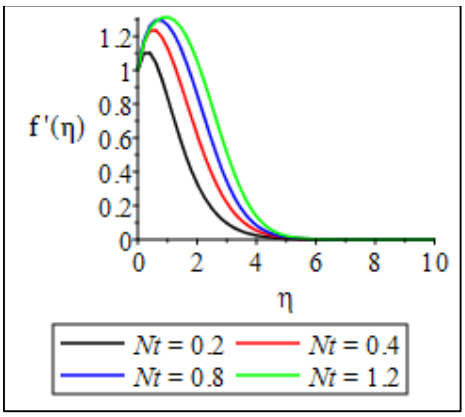

Figure 7: Variation of Velocity Distribution with Thermophoresis parameter

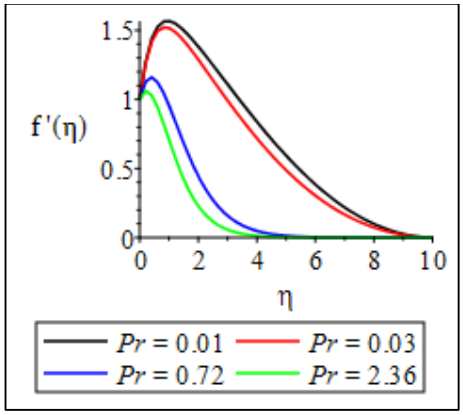

Figure 8: Effect of varying Prandtl number on Velocity Distribution

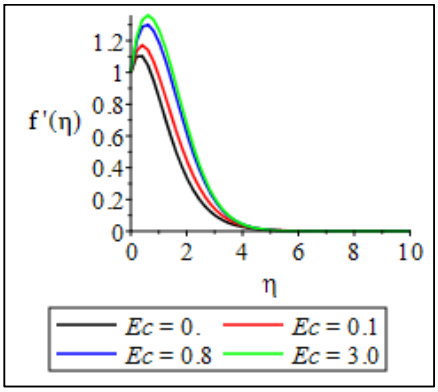

Figure 9: Effect of Eckert number on Velocity Distribution

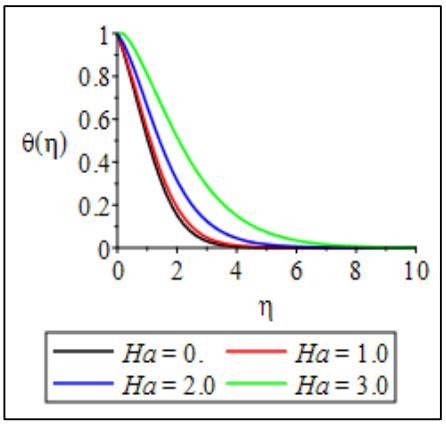

Figure 10: Effect of Hartmann number on Temperature Distribution

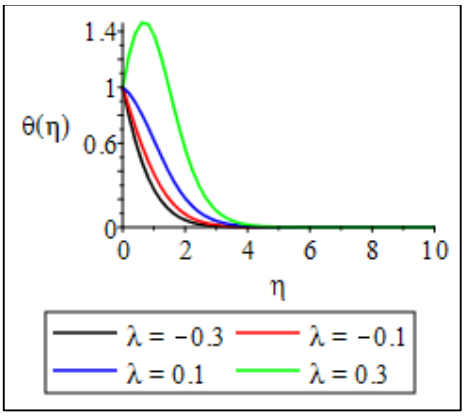

Figure 11: Effect of generation/absorption on Temperature Distribution

Conclusion.

From the Discussion above, the following conclusion were drawn

- Hartman number adversely affect velocity distribution.
- thermal and mass Grashof numbers aid velocity for cooling problem.
- for higher Grashof number, a peak in the profile indicate that maximum velocity occurs in the body of the fluid close to the surface.
- increase in Lorentz force (Hartman number) brings about increase in temperature
- heat absorption into the system increases the bulk temperature whereas heat generation reduces the temperature as a result of heat removal from the system.
- increase in Eckert number increases the temperature with maximum temperature occurring in the body of the fluid at higher values of Eckert number.
- generative chemical reaction ($\delta < 0$) increases the species concentration while destructive chemical reaction ()$\delta > 0$ decrease the concentration as well as the concentration boundary layers.
- Lorentz force (Ha) brings about decrease in skin-friction, Nusselt number and Sherwood number respectively.
- the skin-friction corresponding to active control is higher than that in passive control
- increase in Thermal Grashof number result in increase in skin-friction with active control having higher values than the passive control scenario while the wall heat transfer decline in both active and passive controls.
- thermal Grashof number enhances the wall mass transfer in active control but retard in passive controls.

- Heat generation/absorption, chemical reaction parameter, local Deborah number are observed to enhance mass transfer at the wall, skin-friction, heat and mass transfer at the wall respectively.

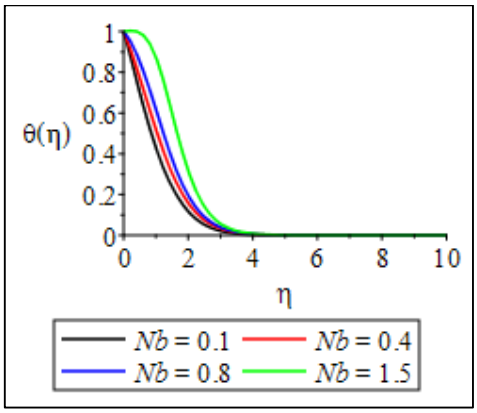

Figure 12: Variation of Temperature distribution with Brownian motion parameter

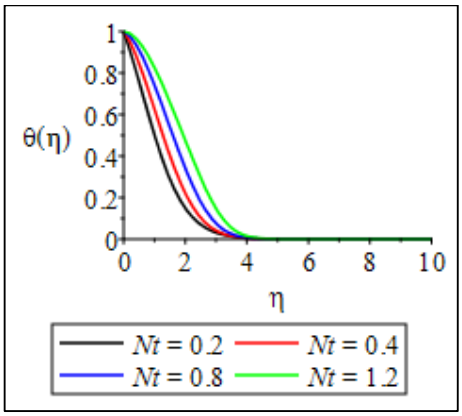

Figure 13: Variation of Temperature Distribution with Thermophoresis parameter

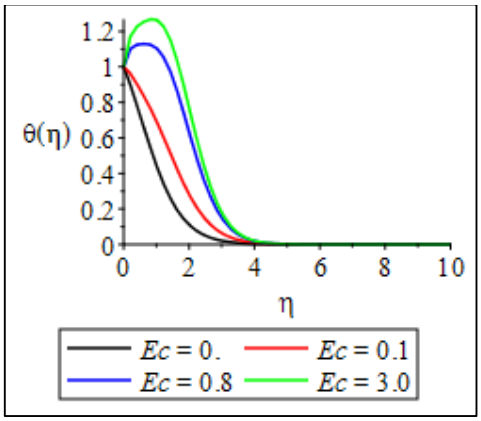

Figure 14: Variation of temperature distribution with Eckert parameter

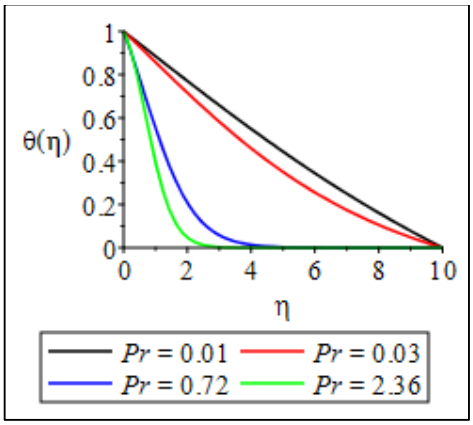

Figure 15: Temperature Distribution with various Prandtl number

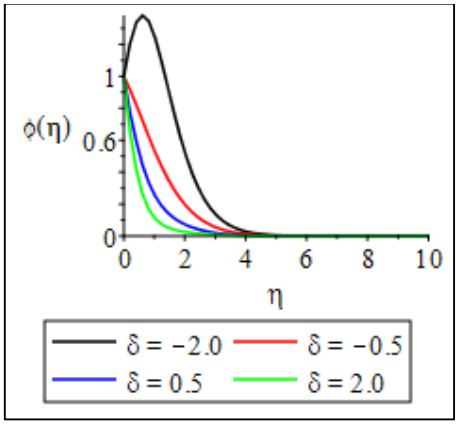

Figure 16: Variation of Species Concentration with reaction parameter

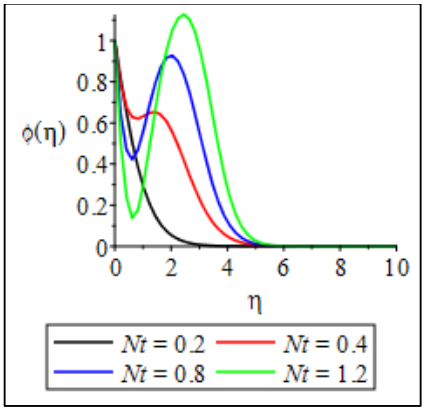

Figure 17: Variation of Species Concentration with Thermophoresis parameter

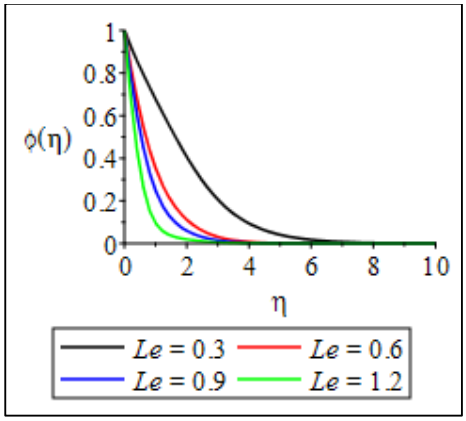

Figure 18: Variation of Species Concentration with Lewis number

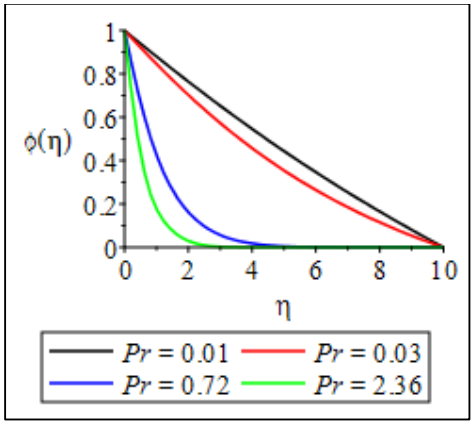

Figure 19: Variation of Species Concentration with Prandtl number

Contribution of Author: Each author made an equal contribution.

Conflict of Interest: According to the authors, there is no conflict of interest.

Acknowledgements:

The management of Covenant University is appreciated and thanked by the writers for providing the conducive environment and research facilities. We also appreciate the anonymous referees' helpful comments, which helped to improve the final product.

Reference

Abbasi FM, Shehzad SA, Hayat T, Alsaedi A, Obid MA. Influence of heat and mass flux conditions in hydromagnetic flow of Jeffrey nanofluid. AIP Adv 2015; 5:037111.

Alsaedi A, Iqbal Z, Mustafa M, Hayat T. Exact solutions for the magnetohydrodynamic flow of a Jeffrey fluid with convective boundary conditions and chemical reaction. Z Naturforsch A 2012;67a:517–24.

Halim NA, Haq RU, Noor NFM. Active and passive controls of nanoparticles in Maxwell stagnation point flow over a slipped stretched surface. Meccanica 2017; 52:1527–39.

Hamad MAA, AbdEl-Gaied SM, Khan WA. Thermal jump effects on boundary layer flow of a Jeffrey fluid near the stagnation point on a stretching/shrinking sheet with variable thermal conductivity. J Fluids 2013;2013:749271.

Hayat T, Abbas T, Ayub M, Muhammad T, Alsaedi A. On squeezed flow of Jeffrey nanofluid between two parallel disks. Appl Sci 2016;6:346.

Hayat T, Aziz A, Muhammad T, Ahmad B. On magnetohydrodynamic flow of second grade nanofluid over a nonlinear stretching sheet. J MagnMagn Mater 2016;408:99–106.

Hayat T, Mahomed FM, Asghar S. Peristaltic flow of a magnetohydrodynamic Johnson-Segalman fluid. Nonlinear Dyn2005;40:375–85.

Hayat T, Qasim M, Mesloub S. MHD flow and heat transfer over permeable stretching sheet with slip conditions. Int J Numer Methods Fluids 2011;66:963–75.

Hayat T, Shehzad SA, Alsaedi A. Soret and Dufour effects on magnetohydrodynamic (MHD) flow of Casson fluid. Appl Math Mech Engl Ed 2012;33:1301–12.

Khan M, Maqbool K, Hayat T. Influence of Hall current on the flows of a generalized Oldroyd-B fluid in a porous space. Acta Mechanica2006;184:1–13.

Kothandapani M, Srinivas S. Peristaltic transport of a Jeffrey fluid under the effect of magnetic field in an asymmetric channel. Int J Non-Linear Mech 2008;43:915–24.

Muhammad T, Hayat T, Alsaedi A, Qayyum A. Hydromagnetic unsteady squeezing flow of Jeffrey fluid between two parallel plates. Chin J Phys 2017;55:1511–22.

Noor NFM, Kechil SA, Hashim I. Simple non-perturbative solution for MHD viscous flow due to a shrinking sheet. Commun Nonlinear Sci. Numer Simul 2010;15:144–8.

Tasawar Hayat, Arsalan Aziz, Taseer Muhammad, Ahmed Alsaedi Active and passive controls of Jeffrey nanofluid flow over a nonlinear stretching surface. Results in Physics 7 (2017) 4071–4078 https://doi.org/10.1016/j.rinp.2017.10.028

Turkyilmazoglu M, Pop I. Exact analytical solutions for the flow and heat transfer near the stagnation point on a stretching/shrinking sheet in a Jeffrey fluid. Int J Heat Mass Transfer 2013;57: 82–8.

Yousefi, Kianoosh; Saleh, Reza (2015-01-23). "Three-dimensional suction flow control and suction jet length optimization of NACA 0012 wing" (PDF). Meccanica. 50 (6): 1481–1494. doi:10.1007/s11012-015-0100-9. ISSN 0025-6455.